HHS Public Access

Author manuscript

Synapse. Author manuscript; available in PMC 2016 July 21.

Published in final edited form as:

Synapse. 2015 May ; 69(5): 268–282. doi:10.1002/syn.21813.

Resolving Presynaptic Structure by Electron Tomography

Guy A. Perkins[1], **Dakota R. Jackson**[2], and **George A. Spirou**[2]

[1]National Center for Microscopy and Imaging Research, University of California, San Diego, San Diego, CA 92092-0608

[2]Center for Neuroscience, Department of Otolaryngology, West Virginia University Morgantown, WV 26506-9303

Abstract

A key goal in neurobiology is to generate a theoretical framework that merges structural, physiological and molecular explanations of brain function. These categories of explanation do not advance in synchrony; advances in one category define new experiments in other categories. For example, the synapse was defined physiologically and biochemically before it was visualized using electron microscopy. Indeed, the original descriptions of synapses in the 1950s were lent credence by the presence of spherical vesicles in presynaptic terminals that were considered to be the substrate for quantal neurotransmission. In the last few decades, our understanding of synaptic function has again been driven by physiological and molecular techniques. The key molecular players for synaptic vesicle structure, mobility and fusion were identified and applications of the patch clamp technique permitted physiological estimation of neurotransmitter release and receptor properties. These advances demand higher resolution structural images of synapses. During the 1990s a second renaissance in cell biology driven by EM was fueled by improved techniques for electron tomography (ET) with the ability to compute virtual images with nm resolution between image planes. Over the last fifteen years, ET has been applied to the presynaptic terminal with special attention to the active zone and organelles of the nerve terminal. In this review, we first summarize the technical improvements that have led to a resurgence in utilization of ET and then we summarize new insights gained by the application of ET to reveal the high-resolution structure of the nerve terminal.

Keywords

electron tomography; cryo ET; active zone; synaptic vesicle; docked vesicle; mitochondrion; crista junction

I. Electron Tomography History and Technologies

Introduction

Published reports show that electron tomography (ET) provides valuable three-dimensional (3D) views of cells, organelles, and macromolecules at resolutions that are useful for

Address Correspondence to: George A. Spirou, Center for Neuroscience, One Medical Center Drive, School of Medicine, Morgantown, WV 26506-9303, t: 304 293-3490, f: 304 293-7182, gspirou@hsc.wvu.edu.

answering questions about cellular functions and mechanisms. ET is the highest resolution 3D technique for investigating pleomorphic structures that cannot be crystallized, such as certain molecules and cellular organelles. What is ET? ET is a method that uses the electron microscope and computer processing for generating 3D images on the basis of multiple 2D projection images of an object, obtained over a wide range of viewing directions, i.e., tilt angles. The 3D reconstruction is generated by using a computer algorithm by back-projecting each 2D image with appropriate weighting (Frank, 1992; Perkins et al., 1997). As such, ET is comparable to the medical imaging method of x-ray computerized axial tomography (CAT) in that it generates projection images to provide a 3D view of an object, yet with nanometer resolution. The 3D perspective it provides has revised our understanding of cellular and organellar organizations, their changes in normal development, and their perturbations due to disease.

A Brief History of ET

The history of ET spans from an early theoretical background, followed by the development of electron microscopy for investigating biological structures beginning in the 1950s, a quantum leap forward in the 1990s with computers powerful enough to generate tomographic reconstructions beyond single particles and isolated organelles, into modern times with its branching into specimen preservation of myriad sample types, genetic labeling, cryo-techniques, and automated data collection, image processing and analyses. The mathematics of tomography was developed almost a century ago with the Radon transform (Radon, 1917). Its first application to biological electron microscopy was on negatively stained single particles (De Rosier and Klug, 1968; Hart, 1968).

The resurgence of ET in the 1990's centered on applications to tissues; the two key technical developments were (1) high-voltage electron microscopes that had eucentric stages and (2) the automation of ET tilt series collection using digital, slow-scan charge-coupled device (CCD) cameras (Koster et al., 1992). There are two flavors of digital image collection. One is with the CCD camera mounted on the microscope itself and the other is with digitizing film, negatives shot on the microscope and developed in a dark room; digitization is done with either a CCD camera or densitometer, the latter often taking an hour or longer per negative. Currently, ET is almost exclusively performed with CCD cameras. A recent advance is marker-free alignment, which has the advantage of not requiring fiducial gold particles on or in the samples (Kim et al., 2013; Winkler and Taylor, 2013). Recent developments allowing large-field electron tomography to be performed enable structural features to be compared that are not near to each other (Berlanga et al., 2011; Phan et al., 2012). Promising current efforts are the development of automatic recognition and segmentation of structural features in tomograms (Mumcuoglu et al., 2012) and identification of specific macromolecular complexes in the rich cellular milieu of cryo-tomograms using subtomogram averaging (e.g., Davies et al., 2014) and template matching (Rigort et al., 2012b; Volkmann 2014).

Much of the current technical development of ET is with cryo-ET, where biological structures are preserved in vitreous ice. Samples prepared in this way are also referred to as being frozen-hydrated. Early techniques are attributable to Fernandez-Moran (1960), who

published cryo-EM of retinal rod, and Christiansen (1971), who developed more accessible procedures to study cryo-EM of pancreas and liver. The development of cryo-EM accelerated with Dubochet and colleagues in the 1980s (Adrian et al., 1984; Dubochet et al., 1988; McDowall et al., 1983). These researchers showed that two advantages of cryo-EM are that (1) rapid freezing can immobilize all molecules in a sample within milliseconds, thus allowing the instantaneous physical fixation of all molecules in their current position, and (2) it produces contrast from the protein density itself and not from a heavy metal stain or replica and allows specimen preservation to atomic detail. The development of high-pressure freezing (HPF) of frozen-hydrated samples followed by cryo-sectioning (Al-Amoudi et al., 2004) has extended this cryo-technique to generate high-quality preservation of cellular architecture, in situ. However, investigators quickly discovered that frozen-hydrated samples had their own challenges, in particular low contrast and susceptibility to electron beam-induced damage. Image processing strategies and low-dose modes of electron microscopy have made progress in overcoming these challenges.

Advances in Tracking Protein Localization via ET

Mini-singlet oxygen generator (miniSOG) is a genetic tag that labels proteins for correlated light and electron microscopy (Shu et al., 2011; Perkins, 2014) and adds to the *in situ* ET protein localization toolbox that also includes immunocytochemical (e.g., Bos et al., 2014; Chen et al., 2008; Linsalata et al., 2014) and template matching tools (Rigort et al., 2012b; Volkmann 2014). MiniSOG provides better structural preservation of cellular components (Cleyrat et al., 2014; Zhou et al., 2013) than conventional immunoEM procedures that use weak fixatives. MiniSOG produces a localized stain through the photo-generated singlet oxygen polymerization of diaminobenzidine (DAB) into an electron opaque osmiophilic precipitate within cells, thus reducing the diffusion of DAB and, as a result, generates a high resolution signal, especially of membrane-associated components. MiniSOG has the additional advantages of being smaller than GFP (106 residues). This new protein-marker strategy will prove useful for correlative LM/ET studies of synaptic signaling dynamics in animals.

An even newer genetic tag for ET protein localization is APEX, a peroxidase enzyme modified from *Arabidopsis* (Hung et al., 2014; Martell et al., 2012; Rhee et al., 2013). It is easier to use than miniSOG because no photo-oxidation is necessary and, like miniSOG, withstands strong EM fixation to provide excellent ultrastructural preservation in combination with localized protein labeling. APEX enzymatically oxidizes DAB in the presence of hydrogen peroxide and, like miniSOG, uses osmication of DAB polymers to contrast the labeled protein. The principal difference between techniques is that miniSOG uses a photoreaction and APEX uses an enzymatic reaction.

The Craft of Cryo-ET

Cryo-ET combines the 3D imaging at up to molecular resolution provided by ET with a close-to-physiological preservation of biological samples using cryo-preservation (recently reviewed in Lucic et al., 2013). The principal challenge in preparing frozen-hydrated samples is freezing them without causing ice crystal damage. The most successful approach is simply to freeze the samples quickly. If the temperature drops rapidly enough, there is

insufficient time for water molecules to contribute to a growing crystal nucleation site before they have lost enough kinetic energy that they no longer move appreciably. The result is vitreous or amorphous (glass-like) ice, a non-crystalline form that does not impose its structure on the biological material it encompasses (Dubochet et al., 1988). Originally, samples had to be less than a few micrometers thick to be frozen without ice crystal damage. These samples were prepared by simply plunging them into liquid ethane or propane, slamming them onto a cold metal mirror, or spraying them with liquid propane (Gilkey and Staehelin, 1986). The idea of using high pressure (about 2000 atmospheres, or bar) to freeze relatively large volumes (up to 200 μm with up to 10 μm depth reliably preserved in neural tissue) without visible ice crystal damage took flight in the mid 1980s when an HPF machine was constructed (Moor, 1987). The increase in usable volume by using HPF comes from preventing water expansion during freezing thus suppressing ice crystal damage deeper inside the sample. Specimens frozen-hydrated by plunge-freezing or by HPF are usually transferred into liquid nitrogen for storage.

The cryo-sectioning of frozen-hydrated samples has provided molecular details of intracellular structures imaged with high clarity. Cryo-sectioning is still far from a routine procedure. The sectioning itself and handling of frozen-hydrated sections is tricky and requires substantial training. Once frozen, the specimens cannot be further manipulated (e.g., by staining or immuno-labeling). Cryo-sections cannot be as thick as plastic sections commonly used for ET and should be kept thinner than about 100 nm to avoid formation of crevasses. Cryo-sectioning is not suitable for serial sectioning because substantial material is lost between each cut, so it cannot produce the image volumes generated by sectioning of plastic sections. Because of its technical challenges in the visualization of molecular structures at high resolution in situ, cryo-sectioning may take a back seat to cryo FIB-SEM (Rigort et al., 2012a), which circumvents several of the challenges mentioned.

Freeze-substitution is a cryo-technique complementary to vitrification. After rapid freezing, the vitrified ice is replaced with chemical fixatives slowly perfused into the sample at low temperature (McDonald and Auer, 2006). Chemical cross-linking happens as the sample slowly is raised to room temperature. At this point, dehydration and plastic embedment follow similarly to conventional EM. Alternatively, cold embedment can be performed using Lowicryl. HPF followed by freeze-substitution is the method of choice currently for examining membrane architecture and cytoskeletal components in a cellular environment because it reduces fixation artifacts and the challenges still facing cryo-sectioning.

Tokuyasu cryo-sectioning is a technique complementary to frozen-hydrated cryo-sectioning that allows the localization of surface-exposed protein épitopes by antibody labeling (Peters et al., 2006). A twist to the Tokuyasu method is taking the immuno-labeled sections and stabilizing them in a thin layer of vitreous water by plunge-freezing prior to cryo-EM (Bos et al., 2014). This vitrification step allows for phase-contrast cryo-imaging. The immunogold labels on the section surface can also be used as fiducial markers for ET alignment.

The Importance of Electron Dose in Cryo-ET

Because frozen-hydrated specimens are very sensitive to the electron beam, radiation damage is the fundamental limiting factor in cryo-ET and the number of electrons used for imaging needs to be minimal (Koster et al., 1992). A typical low-dose imaging scheme is to search for a suitable area at low magnification and thus electron dose. In contrast, accurate focusing is performed at high magnification on a position near the area of interest; the area used for focusing is thus sacrificed and no longer usable. The vast majority of electrons are then used for recording the image. The electron dose that can be used for imaging without loss of high resolution features can be no more than about 100 electrons per square Angstrom. This need for low dose increases the shot noise, which adversely affects the specimen contrast. In an ET tilt series the total dose must be carefully fractionated over all images and thus a lower number of tilts is used. The automated acquisition of electron tomograms is essential to keep the total exposure during ET recording within acceptable limits. As such the angular increments for tilt series collection in cryo-ET is typically 2–3 degrees, whereas for embedded tissue this increment is typically 0.5–1 degrees. This limitation in the number of tilts used in the reconstruction decreases the effective resolution of cryo-ET.

The Resolution of Cryo-ET

High defocus values are used to generate contrast in cryo-ET. Typical defocus values range from −9 to −12 μm, corresponding to the first zero of the contrast transfer function (CTF) at 4.2^{-1} to 4.9^{-1} nm. In essence, the value of the first zero of the CTF is the resolution limit (i.e., 4.2 to 4.9 nm resolution), unless post-processing is performed to account for the CTF. This means that although the resolution of the electron microscope might be excellent, the resolution of reconstructed cells and organelles is currently more limited to about 5–8 nm, depending on the sample thickness, and the robustness of the cryo sample in the electron beam (e.g., see Davies et al., 2014 for an application to mitochondria). The actual resolution can be estimated by Fourier shell correlation using the 0.5 criterion, after splitting the data into two halves (Ibiricu et al., 2011). One way to increase the resolution of cryo-ET is through CTF-correction of tilted images (Xiong et al., 2009). This correction helps to overcome the phase contrast reversal at higher resolutions associated with high-defocus values used to generate contrast. Another way to increase the resolution of ET is through subvolume-averaging of similarly shaped structures, e.g., synaptic vesicles or cytoskeleton, within a highly flexible arrangement of volume elements (Ibiricu et al., 2011; Perkins et al., 2008). Because magnification differences up to a few percent can occur between regions, to improve the resolution of subvolume-averaging, these differences can be compensated for by creating up-scaled or down-scaled maps.

Multiple avenues for technical advances in cryo-ET are being pursued and include recent improvements that are becoming established: (1) controlling the thickness of frozen-hydrated samples by focused ion beam (FIB) milling to complement cryo-sectioning of cells and tissue (Rigort et al., 2012a) and (2) use of direct detection devices (DDDs), which have the advantage of detecting electrons directly, thus avoiding distortions due to the coupling of photons, and which provide a stronger signal and faster readout compared to CCD cameras (Milazzo et al., 2011; Ramachandra et al., 2014). Promising current efforts include: (1) use

of phase plates to partially correct the CTF, which holds the promise of imaging closer to focus and thus extending the resolution before post-processing correction is needed (Danev and Nagayama, 2010); (2) greater use of energy filtering microscopes to allow for thicker samples coupled with improved resolution in cryo-ET (Bouwer et al., 2004) and (3) tilting around two, four or even eight tilt axes to reduce distortions and improve resolution in ET (Figure 1; Mastronarde, 1997). Multi-axis tomography has rarely been used in cryo-ET because of the need to acquire an increased number of tilt images that is a challenge for beam-sensitive samples. The increased sensitivity to electron detection of DDDs and specialized software (Lawrence et al., 2006) is expected to enable the routine use of multi-axis cryo-ET.. Possible future directions include: (1) improvements in cryo-sectioning techniques to eliminate crevasses and increase the usable section thickness and perhaps permit serial sectioning; (2) faster image acquisition and better electron detectors to further minimize the beam-induced damage. Paradoxically, the advantage of cryo-EM to preserve the complete molecular content of a cell significantly complicates the identification of individual molecules or molecular complexes because of the crowded cellular landscape. The development of the new genetic tags miniSOG and APEX for correlative light and electron microscopy are attractive options, especially in combination with FIB-milling cryo-ET, to locate and identify specific proteins in frozen-hydrated samples within large cellular volumes and to add dynamic information from light microscopy to the static tomograms.

II. Applications of Electron Tomography to Nerve Terminal Structure

In this section we report on five structural features of the presynaptic terminal: synaptic vesicles, connectors among synaptic vesicles, docking of synaptic vesicles to the presynaptic membrane, active zone (AZ) dense material apposed to the presynaptic membrane and mitochondria. All of these structures were observed using TEM and, to varying degrees, have altered characteristics when viewed using ET. Furthermore, the higher resolution views afforded by ET have revealed consistencies and differences in elements and organization of the presynaptic cytomatrix based upon tissue immobilization and processing strategies. We consider four general procedures in tissue processing that need not all be brought to bear in a single preparation: aldehyde fixation, dehydration including freeze substitution and/or plastic embedding, staining using a variety of mordants and heavy metals, and vitrification (Tables 1 and 2). In the following discussion we group these procedures generally into combinations that have been employed in most studies: (1) conventional procedures using aldehyde fixation (CAF), dehydration and embedding, tissue staining, (2) vitrification of tissue either by rapid freezing or high pressure freezing (RF/HPF), dehydration by freeze substitution (FS) and embedding, tissue staining and (3) vitrification of tissue either by rapid freezing or high pressure freezing, no dehydration, no tissue staining and imaging by cryo ET. These variable preparations, which we refer to as CAF (after Sosinsky et al. 2008), RF/FS or HPF/FS and cryo ET, respectively, have led to different models for SV docking and interpretation of presynaptic structure. In the following paragraphs we present observations of synaptic terminals by ET in the context of differing methods for tissue preparation.

Synaptic Vesicle Size and Distribution

In TEM, SVs contained within the section can be well-indicated because the circumference of the vesicle profile is the most electron dense. Initial reports that SVs ranged in size from 20–65 nm (Palay, 1956; Gray, 1959) have converged across multiple brain regions and species, with tissue processing mostly utilizing CAF, to a typical range of 40–50 nm (Peters et al., 1991). Curiously, few ET studies have reported synaptic vesicle diameters (mean values reported in Table 1). CAF tissue processing yielded values in mammals for rod bipolar cells (38 nm; Graydon et al., 2014), rod photoreceptors (40 nm; Zampighi et al., 2011) and lamprey reticulospinal terminals (47.8; Gustafsson et al., 2002) that were near and overlapped the typical values, yet larger values were found for motor end plates (55.6 nm; Nagwaney et al., 2009). Similar tissue processing procedures produced relatively small vesicles in frog hair cells (34 nm; Lenzi et al., 1999) and *C. elegans* (also 34 nm; Leitinger et al., 2011). HPF/FS of cultured hippocampal slices yielded SVs with typical diameters (42 nm, Siskou et al., 2013; 45 nm, Imig et al., 2014). Interestingly, SV diameters increased by 3–6 nm in Munc131/2 DKO, SNAP-25 KO and Synaptobrevin-2 KO slices (Imig et al. 2014). Combined HPF/FS with glutaraldehyde (a merge of processing procedures 1 and 2) of *C. elegans* NMJ yielded similar, near typical values (37 nm; Stigloher et al., 2011). In attempt to minimize introduction of artifacts into the tissue structure, synaptosomes from cerebral cortex were prepared and placed onto EM grids, vitrified and studied without dehydration or staining with heavy metals (cryo ET). These procedures yielded SVs also with more typical values (39.5 and 41.5 nm; Fernandez-Busnadiego et al., 2010, 2013). As in other ET KO studies, SV diameter increased in KO of Rim1α, an AZ organizing molecule (Fernandez-Busnadiego et al., 2013). These authors also processed hippocampal slices for cryo ET, but could not perform dimensional measurements on SVs because sectioning of frozen tissues results in an artifact of slice compression in the direction of cutting. Given that SV diameters at mouse NMJ did not vary between CAF or HPF/FS (Nagwaney et al., 2009) and the overlap in results among tissue processing combinations, the variation in reported values by ET may have more to do with species and brain region than method of tissue immobilization and processing.

ET may provide a better estimate of the distribution of SV diameters than TEM, because all vesicles contained within the tissue volume can be reconstructed and those partially contained or those superimposed in the direction of the beam can be readily excluded or distinguished to achieve a less biased sample. Distributions of SV diameters were Gaussian for frog vestibular hair cells (Lenzi et al., 1999) but with small skew to larger values at the lamprey reticulospinal synapse (Gustafsson et al., 2002) (both CAF tissue processing) and *C. elegans* NMJ (Stigloher et al., 2011) (merge of CAF and HPF/FS). Variation in vesicle size is evident in vitrified mouse cortex synaptosome preparations (cryo ET), also with a slight skew to larger diameters (Figure 2B; Fernandez-Busnadiego et al., 2010, 2013). These conglomerate reports with varied tissue processing strategies suggest that vesicles are expected to release differing amounts of neurotransmitter, unless a size filter exists in the docking mechanism, since these distributions included both docked (DV) and undocked vesicles. ET permits a more accurate spatial map of the pool of SVs around each active zone (AZ) and reveals, in synaptosomes imaged by cryo ET, a gap in the alignment of vesicles just behind the row of DVs (Figure 2A, B; Fernandez-Busnadiego et al., 2010, 2013). DVs

may spatially occlude those in the next row, implying a columnar arrangement of SVs in the vesicle halo, since the entire AZ is not occupied by DVs. In HPF//FS hippocampal slices, nerve terminals are larger than when fixed using CAF. As a result, SV density is less and clusters could be identified (Rostaing et al., 2006). Perhaps consistent with these results, periodicity in SV placement was not found at *C. elegans* NMJ (Figure 2C; Stigloher et al., 2011). In general, analysis of SV spatial distribution has not been exploited in other ET studies of the nerve terminal (Table 1).

Connectors among Synaptic Vesicles

Although linkages between SVs were observed during the first three decades of TEM studies (Peters et al., 1991), their 3D characteristics and arrangements and possible protein identity were first revealed by rapid freezing with freeze-fracture etching or freeze substitution (Gotow et al., 1991; Hirokawa et al. 1989; Landis et al., 1988). ET permits investigation of these linkages, which we term “connectors” after Fernandez-Busnadiego et al. (2010), through greater tissue depth (Table 2). Connectors were first described using ET in the lamprey reticulospinal nerve terminal (CAF), where SVs cluster tightly with up to 12 connectors/SV and each of relatively short length up to 15 nm (Gustafsson et al., 2002). Fewer connectors per SV and longer length connectors were found in mammals in other CAF preparations: 2.8 connectors/SV with average length of 32 nm in cat calyx of Held (Perkins et al., 2010) and 3–6 connectors/SV with 10–20 nm length (Figure 3A; Burette et al., 2012). A detailed description of all connectors in a SV halo was performed on rodent hippocampal slice preparations (HPF/FS), revealing an average of 1.5 connectors/SV with an average length of 32 nm. In some instances SVs were nearly adjacent (Figure 3C, D; Siksou et al., 2007). In vitrified synaptosomes from cerebral cortex (cryo ET) there were ~3 connectors/SV with linkages that averaged ~10 nm in length and values up to ~40 nm (Figure 3B; Fernandez-Busnadiego et al., 2010, 2011, 2013). Clusters of SVs could be large (> 50 SVs) or relatively small (< 10 SVs), perhaps with larger clusters located further from the presynaptic membrane (Fernandez-Busnadiego et al., 2010). The fewest connectors (1/SV) but with a more typical length (25.1 nm) were described in *C. elegans* NMJ (merge of CAF and HPF/FS; Stigloher et al., 2011). The existence of connectors across preparations indicates they are not an artifact of any tissue processing procedure (Siksou et al., 2010). The number of connectors/SV and their lengths may depend more on the density of SVs across brain region and species rather than on the methods for tissue processing, noting that densities can be increased by glutaraldehyde fixation (Rostaing et al., 2006). Synapsins are a likely connector element; synapsin TKO mice have fewer SVs per hippocampal bouton with some connectors still present, indicating a complex role in regulation and organization of the SV pool (Siksou et al., 2007). General inspection of tables 1 and 2 reveals the need for more data to compare across preparations and for greater consistency among laboratories in the types of quantification that are reported.

Structure of the Active Zone: Presynaptic Bodies, Synaptic Vesicle Tethers and Dense Proje ctions

Soon after discovery of the synapse in the electron microscope (de Robertis and Bennett, 1955; Palay, 1956, Robertson 1955), it was realized that there were defining and consistent features but also differences among synapse type (Gray, 1959). The presynaptic terminal had

regions where SVs were in direct contact with the presynaptic membrane, electron dense projections that could form a grid that organized SVs at the membrane (Gray, 1963, Bloom and Aghajanian, 1966), or electron dense synaptic bodies that hovered over the presynaptic membrane and bound SVs (Nouvian et al., 2006; tom Dieck and Brandstatter, 2006). In this section, we will discuss the varied appearance of these features based upon methods for sample preparation and review cytoskeletal characteristics at the AZ. We employ terminology whereby a chemical synapse is the functional contact zone for SV fusion and postsynaptic detection and comprises: (1) a presynaptic AZ defined as the region of presynaptic cell membrane where SVs fuse, (2) electron dense material attached to the AZ (which we refer to as AZ material) that can also link to SVs, (3) a synaptic cleft between pre- and postsynaptic membranes and (4) a postsynaptic receptor region appearing in EM as the postsynaptic membrane with an attached electron dense band (postsynaptic density). A nerve terminal may contain one to many AZs along with mitochondria and SV pools. We refer to direct linkages between SVs and the AZ as “tethers” after the terminology of Fernandez-Busnadiego et al. (2010).

Presynaptic bodies, which fall under the general heading of ribbon-class structures based upon their appearance in single TEM sections, are found in sensory cells and neurons of the retina and inner ear (Nouvian et al., 2006; tom Dieck and Brandstatter, 2006). The prevailing view is that synaptic ribbons function to organize and guide SVs en route to the AZ (Lenzi and von Gersdorff, 2001). These structures are termed synaptic bodies in frog saccular hair cells and were first studied using ET by Lenzi et al. (1999, 2002), who confirmed them to be spherical in shape, as suggested by previous TEM studies (Roberts et al., 1990), with average diameter of nearly 500 nm. They lacked internal structure and were positioned over the AZ, about one SV diameter (50 nm) from the presynaptic membrane. SVs coated ~50% of the synaptic body surface, with an average of 376 vesicles linked by 1–2 short filaments that averaged 21 nm in length. The synaptic bodies were linked to dense AZ material and nearly all SVs between the synaptic body and the presynaptic membrane (average 32 SVs) were also in direct contact with the AZ. In some images these SVs were also attached via short tethers to the AZ. The dense AZ material occurred either in bands or patches and was not regular in arrangement. In retina, synaptic ribbons in rod photoreceptors and bipolar cells have been studied using ET (Figure 4A, B; Zampighi et al., 2011; Graydon et al., 2014). Ribbons in photoreceptors were 420 nm tall and 30 nm wide; ribbons in bipolar cells were nearly rectangular with dimensions of 41 nm thickness, extending 135 nm from the presynaptic membrane and 185 nm long. The smaller surface area of bipolar cell ribbons than hair cell synaptic bodies had an average of 35.1 SVs attached by linkages of 29.5 nm length, an average of 8.1 of which were directly apposed to the presynaptic membrane or linked via short tethers (Figure 4A).

ET study of the organization of AZ material and associated SVs in the motor nerve terminal of the frog neuromuscular junction revealed an elaborate, almost crystalline structure (Harlow et al., 2001, Szule et al., 2012). A latticework of pegs, ribs and beams created an elongated structure within 15 nm of the presynaptic membrane with DVs lined in two rows, one along each edge and attached to the ribs. A similar arrangement was found in mouse NMJ, but AZ material forms two rows along the edge of a pair of DVs (Nagwaney et al., 2009). In frog (but not yet investigated in mouse), additional AZ material sits atop this

latticework and extends to about 75 nm from the AZ, from which other linkages emanate called spars and booms, 16–18 nm in length, that also contact SVs (Figure 4C–F). SVs along the latticework that directly contacted the AZ were considered DVs by this criterion. Each DV was contacted by 11 of these conglomerate linkages. DVs were also contacted directly by tethers, called “pins”, which extended from the AZ and averaged 8.6 nm in length. The top of the AZ material, away from the membrane, also contacted SVs. The closer an SV to the AZ material, the more linkages that contacted it in the form of ribs, spars, booms and pins. Following stimulation, the emerging picture was that the AZ material guided SVs to the membrane (Szule et al., 2012), functioning in similar fashion to ribbon-like structures. Application of ET to *Drosophila* NMJ following HPF/FS revealed some similar elements to the frog NMJ (Jiao et al., 2010). A dense core of AZ material sat on short legs over the presynaptic membrane with fibrillar extensions away from the AZ. These extensions contacted SVs, which themselves could be linked by connectors. DVs were contacted by extensions lateral to the central core and were also linked by tethers to the AZ. The T-bar structure seen in CAF TEM was not evident in ET.

AZ material in the form of presynaptic dense projections was first revealed by fixation with osmium alone or in combination with phosphotungstic acid staining and appeared as solid spheres or triangles adhered to the AZ (Gray, 1959, 1963). The subsequent description of grids of dense projections at many CNS synapses, in some cases using other stains such as bismuth iodide (Pfenninger, 1969, 1971), coalesced around a functional interpretation that they organize SVs for membrane fusion (Gray and Willis 1970). From the first application of rapid freezing techniques, however, the possibility that dense projections were artifactual was raised. By rapid freeze-etching of mouse cerebellar slices to a depth of 20–30 nm, networks of filaments were observed surrounding SVs, but without obvious evidence of a condensed organization (Landis et al., 1988). Note that these procedures permitted evaluation of 3D structure, but through limited depth not even extending across the full diameter of a SV. ET permits higher resolution views of dense projections than does TEM and through greater tissue depth than rapid freeze-etching. In CAF specimens from rat neocortex, ET has revealed clumps of AZ material that exhibited an internal organization, called “syndesomes” (Zampighi et al., 2008). Syndesomes were fit to a polyhedral shape, approximately spherical with a diameter of 59 nm, regularly positioned on the AZ and coated by a halo of SVs. SVs contacting the lateral surface were also apposed to the AZ and were defined as DVs. Filaments extended from the syndesomes to contact SVs outside of the immediate vesicle halo. In CAF processed rat cerebral cortex and hippocampus, ET revealed condensed filamentous networks (Figure 4F, G; Burette et al., 2012) that were intermittently present and did not form a regular grid as initially described (Gray, 1963). Where present, they formed a web about 40 nm across the AZ and extended about 60 nm into the nerve terminal, with branching connections to 4–6 SVs. As in other CAF preparations, DVs were defined as SVs apposed to the AZ. These DVs and other SVs near the presynaptic membrane could be linked by short tethers to the AZ (Figure 4F). This conglomerate view of AZ material organizing a halo of SVs, potentially as a guide to a docked state, bears resemblance to proposed function of synaptic ribbons and the AZ grid at the frog NJM.

Processing brain slices by HPF/FS yields a less organized view of the AZ material (Siksou et al. 2007, 2009a,2009b, 2011). As in CAF processed tissue, a DV population was defined as

being apposed to the AZ (Figure 4H, I). Filamentous material extended from the AZ surrounding and contacting DVs, but did not form a condensed network. Elements of this network contacted DVs laterally by short linkages (Siksou et al., 2009), but could also extend to contact SVs further from the membrane via filaments that averaged 82 nm in length (Siksou et al., 2007). Short tethers also linked DVs directly to the AZ membrane (Figure 4H; Siksou et al., 2009). In similarly processed cultured hippocampal neurons, DVs were also apposed to the AZ and linked by short tethers; other vesicles considered to be DVs were depicted within 10 nm of the AZ and connected by tethers (Arthur et al., 2010). The AZ material was not investigated in this study. In an arrangement that differed from other preparations, synaptosomes imaged by cryo ET rarely exhibited SVs apposed to the presynaptic membrane, but did contain a population of vesicles within about 10 nm of the presynaptic membrane that were linked to it by one to several tethers (Figure 4J; Fernandez-Busnadiego et al., 2010, 2013). The number of tethers inversely correlated with distance from the AZ. A diffuse distribution of AZ material was present, but did not appear to surround many SVs (Figure 4K). Based upon these observations, these authors proposed a model for vesicle fusion that defines DVs as those tethered to the AZ and primed DVs as those tethered closely to the AZ by multiple filaments, without the presence of organized, condensed AZ material.

The existing set of ET studies using different methods for tissue preparation provide insight into potential artifactual elements in tomographic image series of synapses. Direct comparison of nerve terminal volume among preparation procedures revealed increasing volume from CAF to HPF/FS to cryo ET, so aldehyde fixation likely condenses intracellular structural elements of the tissue (Rostaing et al., 2006). Aldehyde fixation can lead to SV fusion and neurotransmitter release (Smith and Reese, 1980), although this phenomenon is not prevalent in all brain regions (e.g. calyx of Held terminal, Satzler et al., 2002; cultured hippocampus, Rosenmund and Stevens, 1997). In vitrified synaptosomes, SVs were rarely apposed to the AZ membrane, instead being attached to it via short tethers. It is difficult to envision how rapid freezing would move vesicles away from the membrane, so a consistent effect of aldehyde fixation may be to move SVs from nearby to apposed to the AZ. Likewise, in HPF/FS samples SVs were apposed to the AZ membrane, implying that the dehydration process may shift structures by several nm. Although DVs apposed to the AZ may be artifactual, short tethers, which are a common feature across preparations, are not removed by this potential rearrangement of SVs. Nonetheless, DVs as a morphological indicator of the readily releasable pool (RRP) size of SVs was given credence by rapid stimulation-rapid freezing (freeze several to tens of msec after photo-activation) of cultured neurons (Watanabe et al., 2013). This metric has been utilized in HPF/FS of organotypic hippocampal slices to support an association between DVs and the RRP size, to indicate in KO animals the requirements for the SNARE and SNARE-binding proteins munc13-1/2, SNAP-25, syb-2 and stx-1 in vesicle docking, and to reveal that syt-1 and CPX-1/2/3 are not players in vesicle docking (Imig et al., 2014).

Whether the AZ material is an artifact of aldehyde fixation and/or dehydration is a key issue. It is noteworthy that at the frog NMJ, the crystalline arrangement of AZ material persists in both CAF and HPF/FS preparations, so aldehyde fixation does not dramatically reorganize these structures (Szule et al., 2012). In general, the AZ material at CNS synapses reveals a

filamentous network in both CAF and HPF/FS. Even though the AZ material exhibits less organization by not demonstrating periodicity in higher density in HPF/FS specimens, it does surround and attach to DVs and other SVs near the AZ membrane. In cryo ET, AZ material is present but lacks a coherent spatial relationship to DVs. One must consider potential tissue processing artifacts, including tissue treatment in synaptosome preparation and declining tissue organization in organotypic slices. Given the lower contrast of tissue imaged by cryo ET, one must wonder if an incomplete picture of the AZ material is presented (Sudhof, 2012). Technical improvements that increase the signal to noise ratio, as described in section I of this review, may extract additional information from images and a view of the AZ material that converges toward that presented by other means of tissue preparation. Cryo ET of synaptosomes and CAF or HPF/FS of neuromuscular junction do exhibit a striking similarity in the inverse relationship between number of tethers and distance from the AZ. All techniques may reveal a common mechanism of capturing and docking SVs, embodied in the similar characteristics of a linked halo of vesicles at various distances from the AZ found in synaptic ribbons, latticework at the NMJ and organized or diffuse AZ material in contact with SVs seen at other synapses. Application of cryo ET to ribbon synapses and NMJ will prove very revealing.

ET Characterized the Mitochondrion Associated Adherens Complex

In multiple brain regions, mitochondria take up calibrated positions within nerve terminals facing the membrane and often adjacent to synapses (summarized in Lieberman and Spacek, 1997 and Perkins et al., 2010). These mitochondria appeared to be linked to adherens junctions through filamentous and patchlike electron dense material that often surround a narrow reticulated membrane. In some brain regions (e.g. thalamic relay nuclei) a key characteristic was the emergence of filaments from the presynaptic and often the postsynaptic regions of the adhering junction, so they were called filamentous contacts (Collonier and Guillery, 1964; Lieberman and Spacek, 1997). In its original description in cat dorsal horn (Gray, 1963) and in large nerve terminals of the auditory system (Cant and Morest 1979; Tolbert and Morest 1982; Spirou et al., 1998; Rowland et al., 2000), the presynaptic mitochondrion and in some cases an aligned postsynaptic mitochondrion were defining features of the organelle complex, which was termed the mitochondrion-associated adherens complex (MAC) (Spirou et al., 1998).

MACs in the calyx of Held, perhaps the largest nerve terminal in the mammalian brain, were studied using ET, which revealed lamellar cristae that were linked via crista junctions (Frey and Mannella, 2000; Perkins et al., 1997) to the intermembrane space along the surface of the mitochondrion at higher density facing toward than away from the presynaptic membrane (Figure 5A–G). Note that the discovery of the crista junction was one of the triumphs of ET (Frey and Mannella, 2000; Perkins et al., 1997). The crista junction is a sharply curved membranous neck resembling a T-intersection that has a relatively uniformly sized diameter between 9–20 nm throughout nature. The crista junction architecture may support two forms of functional compartmentation by preventing the mixing of cristae and inner membrane proteins (Davies et al., 2011; Frey et al., 2002; Gilkerson et al., 2003; Pfanner et al., 2014; Vogel et al., 2006; Wurm and Jacobs, 2006) and preventing the mixing or release of soluble proteins that are purposely sequestered within mitochondria (Landes et

al. 2010; Mannella et al., 2013; Scorrano et al., 2002; Yamaguchi et al., 2008). The MAC mitochondria were linked to an adherens junction at the presynaptic membrane via a novel scaffolding system that included struts with thickness slightly greater than intermediate filaments and microfilament linkers to the outer mitochondrial membrane. This unusual polarization of mitochondrial internal structure over a cytoskeletal system tethering the mitochondrion to the presynaptic membrane was proposed to support chemical neurotransmission and perhaps novel modes of non-synaptic communication between synaptic partners (Perkins et al., 2010).

Mitochondria have also been studied using ET in synaptic regions of rod and cone photoreceptors (rod spherules and cone pedicles; Johnson et al., 2007), both of which contain ribbon synapses. Mitochondria in both of these terminal types have primarily tubular cristae, in contrast to MAC mitochondria (Figure 5H–K). The ratio of cristae membrane to outer mitochondrial membrane area is related to metabolic capacity and in rod spherule mitochondria is nearly twice the value of cone pedicle mitochondria and MAC mitochondria (Johnson et al., 2007; Perkins et al., 2010). Synaptic mitochondria exhibit a greater cristae/outer membrane surface area than mitochondria in other neuronal compartments and glia (summarized in Perkins et al., 2010), perhaps reflecting the large energy requirements of nerve terminals (Attwell and Laughlin 2001). This variability in mitochondria placement and cristae structure exemplifies the need to image more brain regions and larger volumes of individual nerve terminal types, using ET, to include all organelles that factor into the dynamics of synaptic transmission.

Summary and Future Directions

ET provides detailed resolution of small tissue volumes, but the nerve terminal is a dynamic system of organelles. Investigation of organelle arrangement and its interface with cytoskeletal and other protein complexes requires ET of thick tissue sections and, ideally, serial sections. CAF and HPF/FS techniques remain superior to cryo-ET in this regard. Even in application to single sections, all techniques induce artifact potentially in both tissue preparation and tissue immobilization. For example, synaptosomal or cultured neuron preparations may introduce artifacts in arrangement of SVs and mitochondria prior to rapid freezing. One test of the cryoET synaptosome preparation would be to examine hippocampal synaptosomes to determine if calibrated positioning of mitochondria nearby AZs in boutons (Spacek and Harris, 1998) maintain their integrity. In this light, new combinations and modifications of techniques that involve fixation, rapid freezing, freeze substitution and staining may result in less rearrangement of molecules and organelles and make accessible deep brain regions that require a time-consuming (i.e., more than a few tens of seconds) surgical approach (e.g. Sosinsky et al., 2008). Much mystery surrounds the guidance of SVs in the halo around the AZ toward the presynaptic membrane, operating at distances beyond interactions among SNARE proteins (~8 nm, Li et al., 2007). ET will increasingly be applied to studies not only of proteins that operate near the AZ (dimensions of ~10 nm) such as Rim1α (Fernandez-Busnadiego et al., 2013) but also at longer distances (up to 100 nm) and via presynaptic structures such as synaptic ribbons, active zone material and crystalline structures at the neuromuscular junction. While KO studies provide important information, mapping with new labels, such as modifications of miniSOG and APEX that require protein

interaction, along with titrated deposition of electron dense markers, would provide more direct reporting of cytomatrix structure surrounding the AZ. It is also apparent that, even in these early days of ET imaging of nervous tissue, a more systematic design among laboratories for image quantification along with consistent, automated techniques for image segmentation will contribute much to our understanding of nerve terminal structure at high resolution. Acquisition of larger image volumes of nerve terminals at high resolution across serial sections and comparison of the same regions of the nervous system using different preparative techniques will shed light on the true variability in synaptic structure first alluded to over fifty years ago (Gray, 1959).

Acknowledgments

This work was supported by NIH/NIDCD Grant R01 DC007695 to GS, NIH/NIGMS CoBRE Grant P30 GM103703 to the WVU Center for Neuroscience and NIH/NIGMS Grant P41 GM103412 to the National Center for Microscopy and Imaging Resources. The authors have no conflict of interest.

References

Adrian M, Dubochet J, Lepault J, McDowall AW. Cryo-electron microscopy of viruses. Nature. 1984; 308:32–36. [PubMed: 6322001]

Al-Amoudi A, Chang JJ, Leforestier A, McDowall A, Salamin LM, Norlen LP, Richter K, Blanc NS, Studer D, Dubochet J. Cryo-electron microscopy of vitreous sections. EMBO J. 2004; 23:3583–3588. [PubMed: 15318169]

Arthur CP, Dean C, Pagratis M, Chapman ER, Stowell MHB. Loss of synaptotagmin IV results in a reduction in synaptic vesicles and a distortion of the Golgi atructure in cultured hippocampal neurons. Neuroscience. 2010; 167:135–142. [PubMed: 20138128]

Attwell D, Laughlin SB. An energy budget for signaling in the grey matter of the brain. J Cereb Blood Flow Metab. 2001; 21:1133–1145. [PubMed: 11598490]

Berlanga ML, Phan S, Bushong EA, Wu S, Kwon O, Phung BS, Lamont S, Terada M, Tasdizen T, Martone ME, Ellisman MH. Three-dimensional reconstruction of serial mouse brain sections: solution for flattening high-resolution large-scale mosaics. Front Neuroanat. 2011; 5:17. [PubMed: 21629828]

Bloom FE, Aghajanian GK. Cytochemistry of synapses: selective staining for electron microscopy. Science. 1966; 154:1575–1577. [PubMed: 5924927]

Bos E, Hussaarts L, van Weering JR, Ellisman MH, de Wit H, Koster AJ. Vitrification of Tokuyasu-style immuno-labelled sections for correlative cryo light microscopy and cryo electron tomography. J Struct Biol. 2014; 186(2):273–82. [PubMed: 24704216]

Bouwer JC, Mackey MR, Lawrence A, Deerinck TJ, Jones YZ, Terada M, Martone ME, Peltier S, Ellisman MH. Automated most-probable loss tomography of thick selectively stained biological specimens with quantitative measurement of resolution improvement. J Struct Biol. 2004; 148:297–306. [PubMed: 15522778]

Burette AC, Lesperance T, Crum J, Martone M, Volkmann N, Ellisman MH, Weinberg RJ. Electron tomographic analysis of synaptic ultrastructure. J Comp Neurol. 2012; 520:2697–2711. [PubMed: 22684938]

Cant NB, Morest DK. The bushy cells in the anteroventral cochlear nucleus of the cat. A study with the electron microscope. Neuroscience. 1979; 4:1925–1945. [PubMed: 530439]

Chen X, Winters C, Azzam R, Li X, Galbraith JA, Leapman RD, Reese TS. Organization of the core structure of the postsynaptic density. Proc Natl Acad Sci U S A. 2008; 105:4453–4458. [PubMed: 18326622]

Christensen AK. Frozen thin sections of fresh tissue for electron microscopy, with a description of pancreas and liver. J Cell Biol. 1971; 51:772–804. [PubMed: 4942776]

Cleyrat C, Darehshouri A, Steinkamp MP, Vilaine M, Boassa D, Ellisman MH, Hermouet S, Wilson BS. Mpl traffics to the cell surface through conventional and unconventional routes. Traffic. 2014; 15:961–982. [PubMed: 24931576]

Colonnier M, Guillery RW. Synaptic organization in the lateral geniculate nucleus of the monkey. Z Zellforsch Mikrosk Anat. 1964; 62:333–355. [PubMed: 14218147]

Danev R, Nagayama K. Phase plates for transmission electron microscopy. Methods Enzymol. 2010; 481:343–369. [PubMed: 20887864]

Davies KM, Daum B, Gold VA, Mühleip AW, Brandt T, Blum TB, Mills DJ, Kühlbrandt W. Visualization of ATP synthase dimers in mitochondria by electron cryo-tomography. J Vis Exp. 2014; 91:51228. [PubMed: 25285856]

Davies KM, Strauss M, Daum B, Kief JH, Osiewacz HD, Rycovska A, Zickermann V, Kühlbrandt W. Macromolecular organization of ATP synthase and complex I in whole mitochondria. Proc Natl Acad Sci USA. 2011; 108(34):14121–6. [PubMed: 21836051]

De Robertis ED, Bennett HS. Some features of the submicroscopic morphology of synapses in frog and earthworm. J Biophys Biochem Cytol. 1955; 1:47–58. [PubMed: 14381427]

De Rosier DJ, Klug A. Reconstruction of three dimensional structures from electron micrographs. Nature. 1968; 217:130–134. [PubMed: 23610788]

Dubochet J, Adrian M, Chang JJ, Homo JC, Lepault J, McDowall AW, Schultz P. Cryo-electron microscopy of vitrified specimens. Q Rev Biophys. 1988; 21:129–228. [PubMed: 3043536]

Fernandez-Busnadiego R, Asano S, Oprisoreanu AM, Sakata E, Doengi M, Kochovski Z, Zurner M, Stein V, Schoch S, Baumeister W, Lucic V. Cryo-electron tomography reveals a critical role of RIM1 in synaptic vesicle tethering. J Cell Biol. 2013; 201:725–740. [PubMed: 23712261]

Fernandez-Busnadiego R, Schrod N, Kochovski Z, Asano S, Vanhecke D, Baumeister W, Lucic V. Insights into the molecular organization of the neuron by cryo-electron tomography. J Electron Microsc (Tokyo). 2011; 60:S137–S148. [PubMed: 21844585]

Fernandez-Busnadiego R, Zuber B, Maurer UE, Cyrklaff M, Baumeister W, Lucic V. Quantitative analysis of the native presynaptic cytomatrix by cryoelectron tomography. J Cell Biology. 2010; 188:145–156.

Fernandez-Moran H. Low-temperature preparation techniques for electron microscopy of biological specimens based on rapid freezing with liquid Helium II. Ann NY Acad Sci. 1960; 85:689–713. [PubMed: 13698977]

Frank, J. Electron Tomography: Three Dimensional Imaging with the Transmission Electron Microscope. Plenum Press; 1992.

Frey TG, Mannella CA. The internal structure of mitochondria. Trends Biochem Sci. 2000; 25:319–324. [PubMed: 10871882]

Frey TG, Renken CW, Perkins GA. Insight into mitochondrial structure and function from electron tomography. Biochim Biophys Acta. 2002; 1555:196–203. [PubMed: 12206915]

Gilkerson RW, Selker JM, Capaldi RA. The cristal membrane of mitochondria is the principal site of oxidative phosphorylation. FEBS Lett. 2003; 546:355–358. [PubMed: 12832068]

Gilkey JC, Staehelin LA. Advances in ultrarapid freezing for the preservation of cellular ultrastructure. J Electron Microsc Tech. 1986; 3:177–210.

Gotow T, Miyaguchi K, Hashimoto PH. Cytoplasmic architecture of the axon terminal: filamentous strands specifically associated with synaptic vesicles. Neuroscience. 1991; 40:587–598. [PubMed: 2027472]

Gray EG. Axo-somatic and axo-dendritic synapses of the cerebral cortex: an electron microscope study. J Anat. 1959; 93:420–433. [PubMed: 13829103]

Gray EG. Electron microscopy of presynaptic organelles of the spinal cord. J Anat. 1963; 97:101. [PubMed: 13949972]

Gray EG, Willis RA. On synaptic vesicles, complex vesicles and dense projections. Brain Res. 1970; 24:149–168. [PubMed: 4099165]

Graydon CW, Zhang J, Oesch NW, Sousa AA, Leapman RD, Diamond JS. Passive Diffusion as a Mechanism Underlying Ribbon Synapse Vesicle Release and Resupply. J Neurosci. 2014; 34:8948–8962. [PubMed: 24990916]

Gustafsson JS, Birinyi AS, Crum J, Ellisman M, Brodin L, Shupliakov O. Ultrastructural organization of lamprey reticulospinal synapses in three dimensions. J Comp Neurol. 2002; 450:167–182. [PubMed: 12124761]

Harlow ML, Ress D, Stoschek A, Marshall RM, McMahan UJ. The architecture of active zone material at the frog's neuromuscular junction. Nature. 2001; 409:479–484. [PubMed: 11206537]

Hart RG. Electron microscopy of unstained biological material: the polytropic montage. Science. 1968; 159:1464–1467. [PubMed: 4183952]

Hirokawa N, Sobue K, Kanda K, Harada A, Yorifuji H. The cytoskeletal architecture of the presynaptic terminal and molecular structure of synapsin 1. J Cell Biol. 1989; 108:111–126. [PubMed: 2536030]

Hung V, Zou P, Rhee HW, et al. Proteomic Mapping of the Human Mitochondrial Intermembrane Space in Live Cells via Ratiometric APEX Tagging. Mol Cell. 2014; 55:332–41. [PubMed: 25002142]

Ibiricu I, Huiskonen JT, Döhner K, Bradke F, Sodeik B, Grünewald K. Cryo electron tomography of herpes simplex virus during axonal transport and secondary envelopment in primary neurons. PLoS Pathog. 2011; 7(12):e1002406. [PubMed: 22194682]

Imig C, Min S-W, Krinner S, Arancillo M, Rosenmund C, Südhof TC, Rhee J, Brose N, Cooper BH. The Morphological and Molecular Nature of Synaptic Vesicle Priming at Presynaptic Active Zones. Neuron. 2014; 84:416–431. [PubMed: 25374362]

Jiao W, Masich S, Franzen O, Shupliakov O. Two pools of vesicles associated with the presynaptic cytosolic projection in *Drosophila* neuromuscular junction. J Struct Biol. 2010; 172:389–394. [PubMed: 20678577]

Johnson JE, Perkins GA, Giddabasappa A, Chaney S, Xiao W, White AD, Brown JM, Waggoner J, Ellisman MH, Fox DA. Spatiotemporal regulation of ATP and Ca2+ dynamics in vertebrate rod and cone ribbon synapses. Mol Vis. 2007; 13:887–919. [PubMed: 17653034]

Kim HW, Oh SH, Kim N, Nakazawa E, Rhyu IJ. Rapid method for electron tomographic reconstruction and three-dimensional modeling of the murine synapse using an automated fiducial marker-free system. Microsc Microanal. 2013; 19(Suppl 5):182–7. [PubMed: 23920202]

Koster AJ, Chen H, Sedat JW, Agard DA. Automated microscopy for electron tomography. Ultramicroscopy. 1992; 46:207–227. [PubMed: 1481272]

Landes T, Leroy I, Bertholet A, Diot A, Khosrobakhsh F, Daloyau M, Davezac N, Miquel MC, Courilleau D, Guillou E, Olichon A, Lenaers G, Arnauné-Pelloquin L, Emorine LJ, Belenguer P. OPA1 (dys)functions. Semin Cell Dev Biol. 2010; 21(6):593–598. [PubMed: 20045077]

Landis DM, Hall AK, Weinstein LA, Reese TS. The organization of cytoplasm at the presynaptic active zone of a central nervous system synapse. Neuron. 1988; 1:201–209. [PubMed: 3152289]

Lawrence A, Bouwer JC, Perkins G, Ellisman MH. Transform based backprojection for volume reconstruction of large format electron microscope tilt series. J Struct Biol. 2006; 154:144–167. [PubMed: 16542854]

Leitinger G, Masich S, Neumüller J, Pabst MA, Pavelka M, Rind FC, Shupliakov O, Simmons PJ, Kolb D. Structural organization of the presynaptic density at identified synapses in the locust central nervous system. J Comp Neurol. 2011; 520:384–400. [PubMed: 21826661]

Lenzi D, Crum J, Ellisman MH, Roberts WM. Depolarization redistributes synaptic membrane and creates a gradient of vesicles on the synaptic body at a ribbon synapse. Neuron. 2002; 36:649–659. [PubMed: 12441054]

Lenzi D, Gersdorff von H. Structure suggests function: the case for synaptic ribbons as exocytotic nanomachines. Bioessays. 2001; 23:831–840. [PubMed: 11536295]

Lenzi D, Runyeon JW, Crum J, Ellisman MH, Roberts WM. Synaptic vesicle populations in saccular hair cells reconstructed by electron tomography. J Neurosci. 1999; 19:119–132. [PubMed: 9870944]

Li F, Pincet F, Perez E, Eng WS, Melia TJ, Rothman JE, Tareste D. Energetics and dynamics of SNAREpin folding across lipid bilayers. Nat Struct Mol Biol. 2007; 14:890–896. [PubMed: 17906638]

Lieberman AR, Spacek J. Filamentous contacts: the ultrastructure and three-dimensional organization of specialized non-synaptic interneuronal appositions in thalamic relay nuclei. Cell Tissue Res. 1997; 288:43–57. [PubMed: 9042771]

Linsalata AE, Chen X, Winters CA, Reese TS. Electron tomography on γ-aminobutyric acid-ergic synapses reveals a discontinuous postsynaptic network of filaments. J Comp Neurol. 2014; 522:921–936. [PubMed: 23982982]

Lučič V, Rigort A, Baumeister W. Cryo-electron tomography: the challenge of doing structural biology in situ. J Cell Biol. 2013; 202(3):407–19. [PubMed: 23918936]

Mannella CA, Lederer WJ, Jafri MS. The connection between inner membrane topology and mitochondrial function. J Mol Cell Cardiol. 2013; 62:51–7. [PubMed: 23672826]

Martell JD, Deerinck TJ, Sancak Y, Poulos TL, Mootha VK, Sosinsky GE, et al. Engineered ascorbate peroxidase as a genetically encoded reporter for electron microscopy. Nat Biotechnol. 2012; 30:1143–1148. [PubMed: 23086203]

Mastronarde DN. Dual-axis tomography: an approach with alignment methods that preserve resolution. J Struct Biol. 1997; 120(3):343–52. [PubMed: 9441937]

McDonald KL, Auer M. High-pressure freezing, cellular tomography, and structural cell biology. Biotechniques. 2006; 41(2):137, 139, 141. [PubMed: 16925014]

McDowall AW, Chang JJ, Freeman R, Lepault J, Walter CA, Dubochet J. Electron microscopy of frozen hydrated sections of vitreous ice and vitrified biological samples. J Microsc. 1983; 131:1–9. [PubMed: 6350598]

Milazzo AC, Cheng A, Moeller A, Lyumkis D, Jacovetty E, Polukas J, Ellisman MH, Xuong NH, Carragher B, Potter CS. Initial evaluation of a direct detection device detector for single particle cryo-electron microscopy. J Struct Biol. 2011; 176(3):404–8. [PubMed: 21933715]

Moor, H. Theory and practice of high pressure freezing. In: Steinbrecht, RA.; Zierold, K., editors. Cryotechniques in Biological Electron Microscopy. Springer-Verlag; Berlin: 1987. p. 175-191.

Mumcuoglu EU, Hassanpour R, Tasel SF, Perkins G, Martone M, Gurcan MN. Computerized Detection and Segmentation of Mitochondria on Electron Microscope Images. J Microscopy. 2012; 246:248–65.

Nagwaney S, Harlow ML, Jung JH, Szule JA, Ress D, Xu J, Marshall RM, McMahan UJ. Macromolecular connections of active zone material to docked synaptic vesicles and presynaptic membrane at neuromuscular junctions of mouse. J Comp Neurol. 2009; 513:457–468. [PubMed: 19226520]

Nouvian R, Beutner D, Parsons TD, Moser T. Structure and Function of the Hair Cell Ribbon Synapse. J Membrane Biol. 2006; 209:153–165. [PubMed: 16773499]

Palay SL. Synapses in the central nervous system. J Cell Biol. 1956; 2:193–202.

Perkins G. The use of miniSOG in the localization of mitochondrial proteins. Methods in Enzymology. 2014; 547:165–79. [PubMed: 25416358]

Perkins G, Renken C, Song JY, Frey TG, Young S, Lamont S, Martone M, Lindsey S, Frey T, Ellisman M. Electron tomography of large, multicomponent biological structures. J Struct Biol. 1997; 120:219–227. [PubMed: 9441927]

Perkins GA, Sosinsky GE, Ghassemzadeh S, Perez A, Jones Y, Ellisman MH. Electron tomographic analysis of cytoskeletal cross-bridges in the paranodal region of the node of Ranvier in peripheral nerves. J Struct Biol. 2008; 161:469–480. [PubMed: 18096402]

Perkins GA, Tjong J, Brown JM, Poquiz PH, Scott RT, Kolson DR, Ellisman MH, Spirou GA. The micro-architecture of mitochondria at active zones: Electron tomography reveals novel anchoring scaffolds and cristae structured for high rate metabolism. J Neurosci. 2010; 30:1015–1026. [PubMed: 20089910]

Peters PJ, Bos E, Griekspoor A. Cryo-immunogold electron microscopy. Curr Protoc Cell Biol. 2006; Chapter 4(Unit 4.7)

Peters, A.; Palay, S.; Webster, HD. The fine structure of the nervous system: neurons and their supporting cells. 3. New York: Oxford; 1991.

Pfanner N, van der Laan M, Amati P, Capaldi RA, Caudy AA, Chacinska A, Darshi M, Deckers M, Hoppins S, Icho T, Jakobs S, Ji J, Kozjak-Pavlovic V, Meisinger C, Odgren PR, Park SK, Rehling P, Reichert AS, Sheikh MS, Taylor SS, Tsuchida N, van der Bliek AM, van der Klei IJ, Weissman

JS, Westermann B, Zha J, Neupert W, Nunnari J. Uniform nomenclature for the mitochondrial contact site and cristae organizing system. J Cell Biol. 2014; 204:1083–1086. [PubMed: 24687277]

Pfenninger K, Sandri C, Akert K, Eugster CH. Contribution to the problem of structural organization of the presynaptic area. Brain Research. 1969; 12:10–18. [PubMed: 4184686]

Pfenninger KH. The cytochemistry of synaptic densities. II. Proteinaceous components and mechanism of synaptic connectivity. J Ultrastruct Res. 1971; 35:451–475. [PubMed: 4111038]

Phan S, Lawrence A, Molina T, Lanman J, Berlanga M, Terada M, Kulungowski A, Obayashi J, Ellisman M. TxBR montage reconstruction for large field electron tomography. J Struct Biol. 2012; 180(1):154–64. [PubMed: 22749959]

Radon J. Uber die bestimmung von Funktionen durch ihre Integralwerte langs gewiser Mannigfaltigkeiten. Ber Sachs Akad Wiss Leipzig Math-Phys Kl. 1917; 69:262–277.

Ramachandra R, Bouwer JC, Mackey MR, Bushong E, Peltier ST, Xuong NH, Ellisman MH. Improving signal to noise in labeled biological specimens using energy-filtered TEM of sections with a drift correction strategy and a direct detection device. Microsc Microanal. 2014; 20(3):706–14. [PubMed: 24641915]

Rhee HW, Zou P, Udeshi ND, et al. Proteomic mapping of mitochondria in living cells via spatially restricted enzymatic tagging. Science. 2013; 339:1328–31. [PubMed: 23371551]

Rigort A, Bäuerlein, Villa E, Eibauer M, Laugks T, Baumeister W, Plitzko JM. Focused ion beam micromachining of eukaryotic cells for cryoelectron tomography. Proc Natl Acad Sci USA. 2012a; 109:4449–4454. [PubMed: 22392984]

Rigort A, Günther D, Hegerl R, Baum D, Weber B, Prohaska S, Medalia O, Baumeister W, Hege HC. Automated segmentation of electron tomograms for a quantitative description of actin filament networks. J Struct Biol. 2012b; 177:135–144. [PubMed: 21907807]

Roberts WM, Jacobs RA, Hudspeth AJ. Colocalization of ion channels involved in frequency selectivity and synaptic transmission at presynaptic active zones of hair cells. J Neurosci. 1990; 10:3664–3684. [PubMed: 1700083]

Robertson JDJ. Recent electron microscope observations on the ultrastructure of the crayfish median-to-motor giant synapse. Exp Cell Res. 1955; 8:226–229. [PubMed: 14353119]

Rosenmund C, Stevens CF. The rate of aldehyde fixation of the exocytotic machinery in cultured hippocampal synapses. J Neurosci Methods. 1997; 76:1–5. [PubMed: 9334932]

Rostaing P, Real E, Siksou L, Lechaire J-P, Boudier T, Boeckers TM, Gertler F, Gundelfinger ED, Triller A, Marty S. Analysis of synaptic ultrastructure without fixative using high-pressure freezing and tomography. Eur J Neurosci. 2006; 24:3463–3474. [PubMed: 17229095]

Rowland KC, Irby NK, Spirou GA. Specialized synapse-associated structures within the calyx of Held. J Neurosci. 2000; 20:9135–9144. [PubMed: 11124991]

Sätzler K, Söhl LF, Bollmann JH, Borst JGG, Frotscher M, Sakmann B, Lübke JHR. Three-dimensional reconstruction of a calyx of Held and its postsynaptic principal neuron in the medial nucleus of the trapezoid body. J Neurosci. 2002; 22:10567–10579. [PubMed: 12486149]

Scorrano L, Ashiya M, Buttle K, et al. A distinct pathway remodels mitochondrial cristae and mobilizes cytochrome c during apoptosis. Dev Cell. 2002; 2(1):55–67. [PubMed: 11782314]

Shu X, Lev-Ram V, Deerinck TJ, Qi Y, Ramko EB, Davidson MW, et al. A genetically encoded tag for correlated light and electron microscopy of intact cells, tissues, and organisms. PLoS Biology. 2011; 9:e1001041. [PubMed: 21483721]

Siksou L, Rostaing P, Lechaire JP, Boudier T, Ohtsuka T, Fejtova A, Kao HT, Greengard P, Gundelfinger ED, Triller A, Marty S. Three-Dimensional Architecture of Presynaptic Terminal Cytomatrix. J Neurosci. 2007; 27:6868–6877. [PubMed: 17596435]

Siksou L, Silm K, Biesemann C, Nehring RB, Wojcik SM, Triller A, Mestikawy El S, Marty S, Herzog E. A role for vesicular glutamate transporter 1 in synaptic vesicle clustering and mobility. Eur J Neurosci. 2013; 37:1631–1642. [PubMed: 23581566]

Siksou L, Triller A, Marty S. An emerging view of presynaptic structure from electron microscopic studies. J Neurochem. 2009a; 108:1336–1342. [PubMed: 19154334]

Siksou L, Triller A, Marty S. Ultrastructural organization of presynaptic terminals. Curr Opin Neurobiol. 2010; 21:261–268. [PubMed: 21247753]

Siskou L, Varoqueaux F, Pascual O, Triller A, Brose N, Marty S. A common colecular basis for membrane docking and functional priming of synaptic vesicles. Eur J Neurosci. 2009b; 30:49–56. [PubMed: 19558619]

Smith JE, Reese TS. Use of aldehyde fixatives to determine the rate of synaptic transmitter release. J Exp Biol. 1980; 89:19–29. [PubMed: 6110693]

Sosinsky GE, Crum J, Jones YZ, Lanman J, Smarr B, Terada M, Martone ME, Deerinck TJ, Johnson JE, Ellisman MH. The combination of chemical fixation procedures with high pressure freezing and freeze substitution preserves highly labile tissue ultrastructure for electron tomography applications. J Struct Biol. 2008; 161:359–371. [PubMed: 17962040]

Spacek J, Harris KM. Three-dimensional organization of cell adhesion junctions at synapses and dendritic spines in area CA1 of the rat hippocampus. J Comp Neurol. 1998; 393:58–68. [PubMed: 9520101]

Spirou GA, Rowland KC, Berrebi AS. Ultrastructure of neurons and large synaptic terminals in the lateral nucleus of the trapezoid body of the cat. J Comp Neurol. 1998; 398:257–272. [PubMed: 9700570]

Stigloher C, Zhan H, Zhen M, Richmond J, Bessereau JL. The Presynaptic Dense Projection of the Caenorhabiditis elegans Cholinergic Neuromuscular Junction Localizes Synaptic Vesicles at the Active Zone through SYD-2/Liprin and UNC-10/RIM-Dependent Interactions. J Neurosci. 2011; 31:4388–4396. [PubMed: 21430140]

Sudhof T. The Presynaptic Active Zone. Neuron. 2012; 75:11–25. [PubMed: 22794257]

Szule JA, Harlow ML, Jung JH, De-Miguel FF, Marshall RM, McMahan UJ. Regulation of Synaptic Vesicle Docking by Different Classes of Macromolecules in Active Zone Material. PLoS One. 2012; 7:e33333. [PubMed: 22438915]

Tolbert LP, Morest DK. The neuronal architecture of the anteroventral cochlear nucleus of the cat in the region of the cochlear nerve root: electron microscopy. Neuroscience. 1982; 7:3053–3067. [PubMed: 7162626]

tom Dieck S, Brandstätter JH. Ribbon synapses of the retina. Cell Tissue Res. 2006; 326:339–346. [PubMed: 16775698]

Vogel F, Bornhövd C, Neupert W, Reichert AS. Dynamic subcompartmentalization of the mitochondrial inner membrane. J Cell Biol. 2006; 175:237–247. [PubMed: 17043137]

Volkmann N. The joys and perils of flexible fitting. Adv Exp Med Biol. 2014; 805:137–155. [PubMed: 24446360]

Watanabe S, Rost BR, Camacho-Pérez M, Davis MW, Söhl-Kielczynski B, Rosenmund C, Jorgensen EM. Nature. 2013; 504:242–247. [PubMed: 24305055]

Winkler H, Taylor KA. Marker-free dual-axis tilt series alignment. J Struct Biol. 2013; 182(2):117–24. [PubMed: 23435123]

Wurm CA, Jakobs S. Differential protein distributions define two sub-compartments of the mitochondrial inner membrane in yeast. FEBS Lett. 2006; 580:5628–5634. [PubMed: 16997298]

Xiong Q, Morphew MK, Schwartz CL, Hoenger A, Mastronarde DN. CTF determination and correction for low dose tomographic tilt series. J Struct Biol. 2009; 168:378–387. [PubMed: 19732834]

Yamaguchi R, Lartigue L, Perkins G, Scott RT, Dixit A, Ellisman MH, Kuwana T, Newmeyer DD. Opa1-Mediated Cristae Opening Is Bax/Bak and BH3 Dependent, Required for Apoptosis, and Independent of Bak Oligomerization. Mol Cell. 2008; 31:557–569. [PubMed: 18691924]

Zampighi GA, Fain N, Zampighi LM, Cantele F, Lanzavecchia S, Wright EM. Conical Electron Tomography of a Chemical Synapse: Polyhedral Cages Dock Vesicles to the Active Zone. J Neurosci. 2008; 28:4151–4160. [PubMed: 18417694]

Zampighi GA, Schietroma C, Zampighi LM, Woodruff M, Wright EM, Brecha NC. Conical Tomography of a Ribbon Synapse: Structural Evidence for Vesicle Fusion. PLoS One. 2011; 6:e16944. [PubMed: 21390245]

Zhou K, Stawicki TM, Goncharov A, Jin Y. Position of UNC-13 in the active zone regulates synaptic vesicle release probability and release kinetics. Elife. 2013; 2:e01180. [PubMed: 24220508]

Zick M, Rabl R, Reichert AS. Cristae formation-linking ultrastructure and function of mitochondria. Biochim Biophys Acta. 2009; 1793(1):5–19. [PubMed: 18620004]

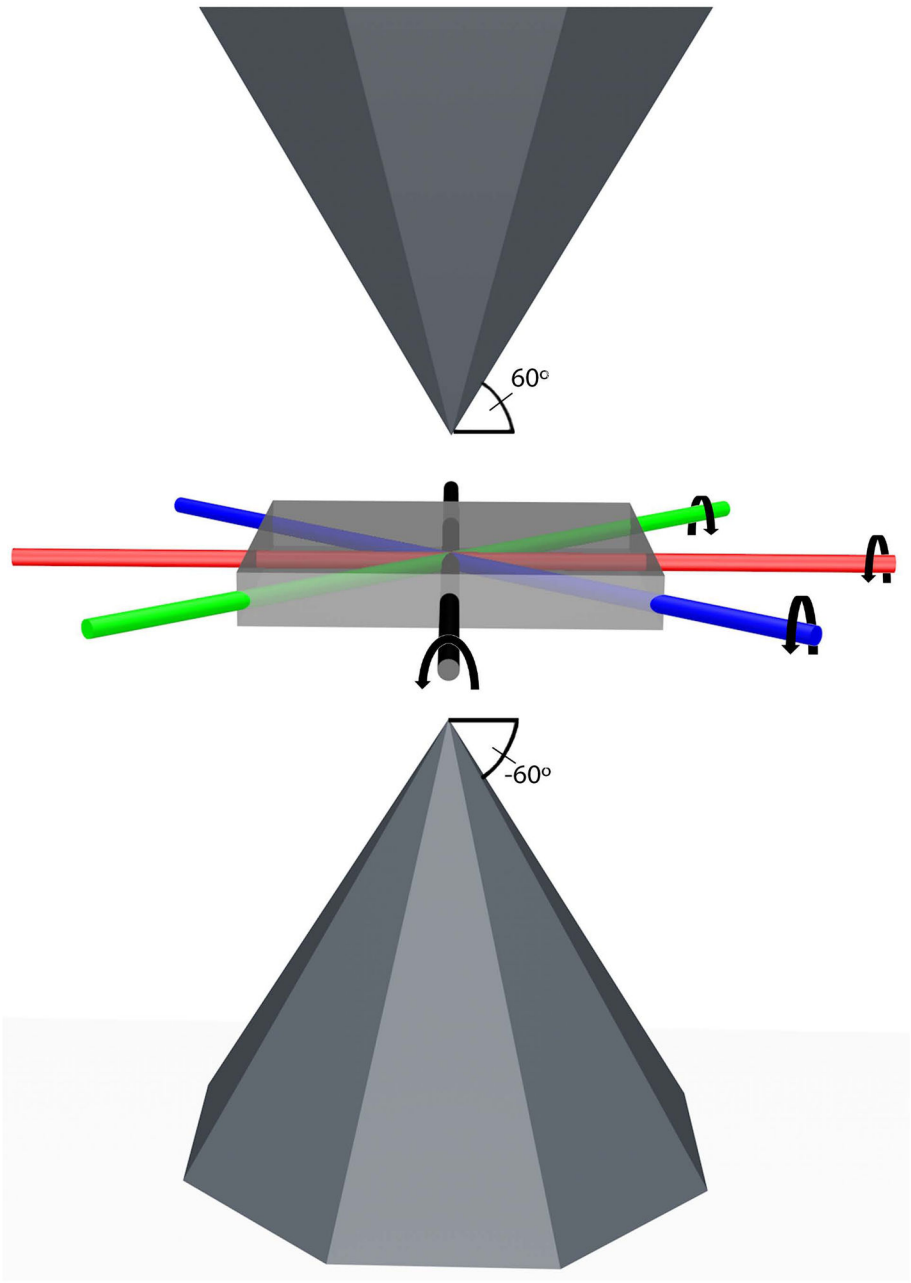

Figure 1. Multi-tilt axis imaging

Imaging of tissue through tilt angles of typically ± 60° results in a range of perspectives that are not sampled. For single axis tilt series the unsampled perspectives are represented by a wedge of space (not depicted) above and below the tissue. Adding additional tilt axes (four are depicted by the colored tubes) reduces the volume of unsampled perspectives and increases the resolution of the reconstructed tomographic series. Four tilt axes, differing by 45° rotation in the plane of the tissue, are depicted by the colored rods through the tissue, which is depicted as a rectangular box. During the tilt series the tissue is rotated eucentrically around each axis through the same angular range. The unsampled image perspectives is reduced from a wedge (single tilt series) to the region represented by the

octagonal pyramids above and below the tissue. Pyramid vertices are displaced away from the tissue for clarity.

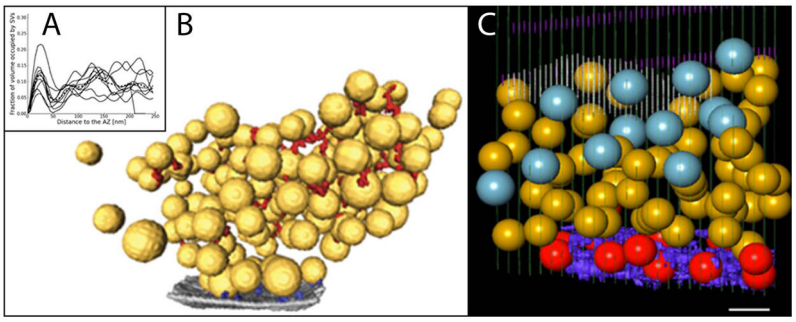

Figure 2. Synaptic vesicle arrangement over the active zone

(A). 3D distribution of synaptic vesicles (SV; gold) over an active zone (AZ) in vitrified synaptosomes. Tethers (blue) from SVs to the AZ and connectors between SVs (red) reveal an interconnected network. **(A').** Histogram of SV location reveals gap in SV placement behind docked vesicles (DV), defined as tethered to the AZ. SV position indicated by center of its sphere. Dotted trace is average of all SV clouds. SVs exhibit variation in diameter and volume. Adapted from Fernandez-Busnadiego et al. (2013). **(B).** 3D distribution of SVs (spheres) over an AZ at *C. elegans* NMJ. DVs (red) are apposed to the AZ and surrounded by AZ material (purple). The vesicle cloud is also comprised of non-docked SVs (gold) and dense-cored vesicles (light blue). Adapted from Stigloher et al. (2011). Scale bar 50 nm.

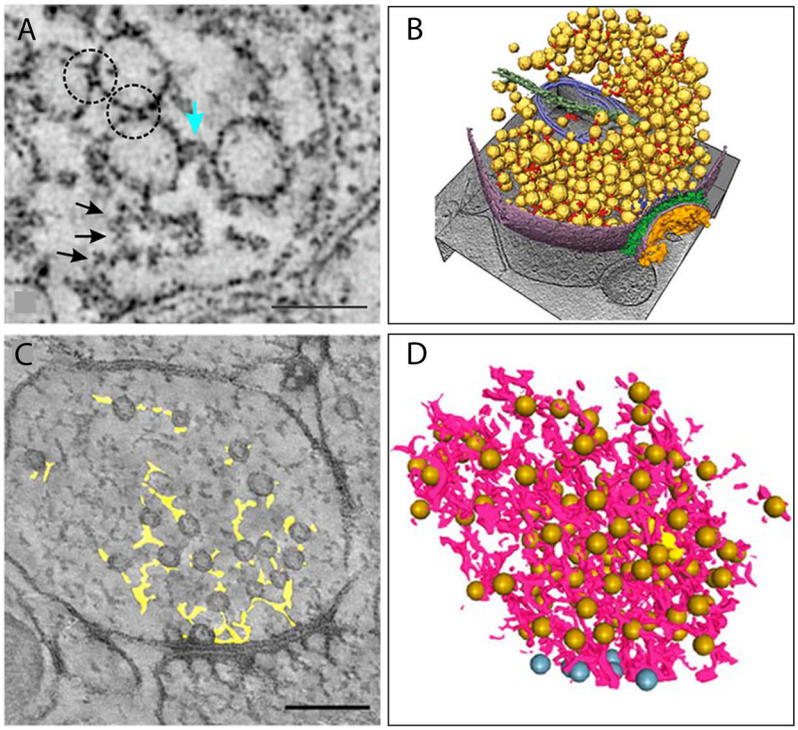

Figure 3. Networks of filaments that link synaptic vesicles found across methods for tissue preparation

(A). SVs are directly apposed (dotted circles) or linked by connectors (cyan arrow). A longer filament (black arrows) links an SV to AZ material and eventually to the AZ. Conventional aldehyde fixation (CAF) tissue preparation prior to ET. Scale bar 50 nm. Adapted from Burette et al., 2012. **(B).** 3D image of SV cloud over a virtual slice from the tomographic series depicts connectors (red) among SVs (gold). A microtubule passes through the SV cloud but distant from the AZ, whose location is indicated by synaptic cleft material (green) and the postsynaptic density (orange). Synaptosome membrane indicated in purple. Cryo-ET of vitrified, non-dehydrated, unstained tissue. Adapted from Fernandez-Busnadiego et al. 2011. **(C).** Virtual slice with segmented connectors and AZ material (yellow) and **(D)** 3D image of SV (gold) cloud depicting the entire cytomatrix (red) of a hippocampal bouton. High-pressure frozen, freeze-substituted tissue prior to ET. Scale bar 200 nm. (D) 3D representation of a reconstructed image volume emphasizing the complexity of the filamentous network linking SVs near the AZ. SV (gold), docked vesicles (blue), filaments (pink). (C–D) Adapted from Siksou et al. 2007.

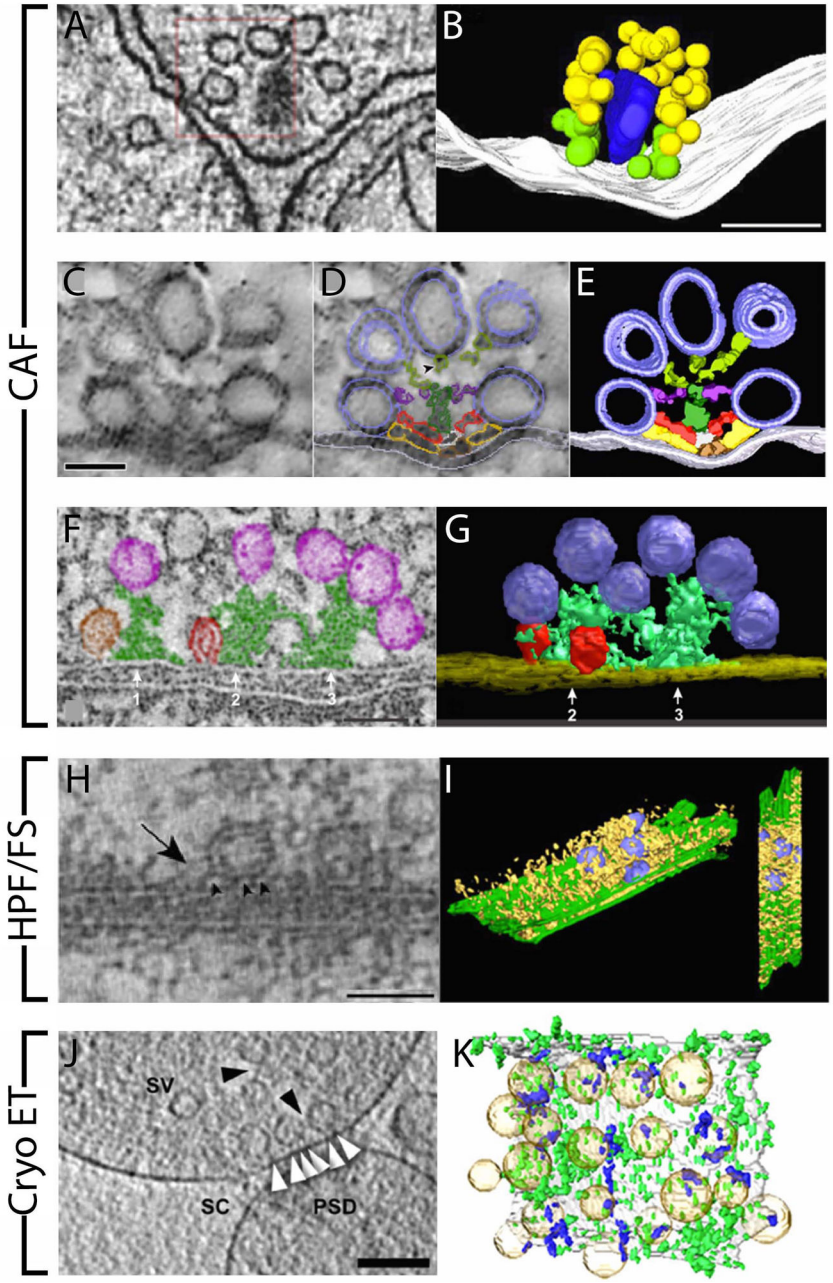

Figure 4. Synaptic vesicles, tethers and active zone material

(A). Virtual section of rat rod bipolar ribbon synapse. Ribbons is oval electron dense object with SV halo. SVs inside red box linked to ribbon; SV at left also has two tethers linking it to the AZ and is considered to be a DV. **(B).** 3D reconstruction of the ribbon shown in A. Ribbon (blue), presynaptic membrane (white), DVs (green), other SVs linked to ribbon (yellow). CAF tissue preparation. Scale bar 250 nm. Adapted from Graydon et al. (2014). **(C–E).** Frog NMJ showing multiple linkers between AZ material and SVs (blue). Virtual slice in A shown segmented in B with 3D reconstruction of eight 1.2 nm thick serial virtual sections in C (ribs, yellow; spars, red; booms, purple; topmasts, light green). DVs are at

either side of AZ material apposed to AZ membrane (white) and also linked by short tethers (called pins, not shown). CAF tissue preparation prior to ET. Scale bar 50 nm. Adapted from Szule et al. (2012). **(F).** Virtual section of hippocampal synapse. AZ material (green) surrounded by SV halo. AZ material links to DV (brown) apposed to AZ, omega-profile of SV with membrane fused to AZ (red) and non-docked SVs (purple). SV at right tethered to AZ. **(G).** 3D reconstruction of the image volume that includes the section depicted in F. Color scheme is consistent with panel F. CAF tissue preparation prior to ET. Adapted from Burette et al. (2012). **(H).** Virtual section of hippocampal synapse showing SV tethered to AZ. DVs in this preparation defined as being apposed to AZ. AZ material evident lateral to SV and connected to SV (arrow). **(I).** 3D reconstruction (side and top views) reveals DVs (purple) apposed to the presynaptic membrane (green) and surrounded by AZ material (gold). AZ material does not form obvious clusters. HPF/FS tissue preparation. Scale bar 50 nm. Adapted from Siksou et al. (2009). **(J).** Virtual section through mouse cortical synaptosome showing SVs tethered (white arrowheads) to AZ. Connectors between SVs (black arrowheads) were prevalent. Postsynaptic density (PSD), synaptic cleft (SC), synaptic vesicle (SV). Scale bar 100 nm. Adapted from Fernandez-Busnadiego et al. (2013). **(K).** 3D view of synaptosome AZ (gray) viewed from presynaptic cytoplasm. AZ material (green) shows regions of condensation but not in consistent relationship to DVs (gold), defined as tethered (blue) to the AZ. Adapted from Fernandez-Busnadiego et al. (2010).

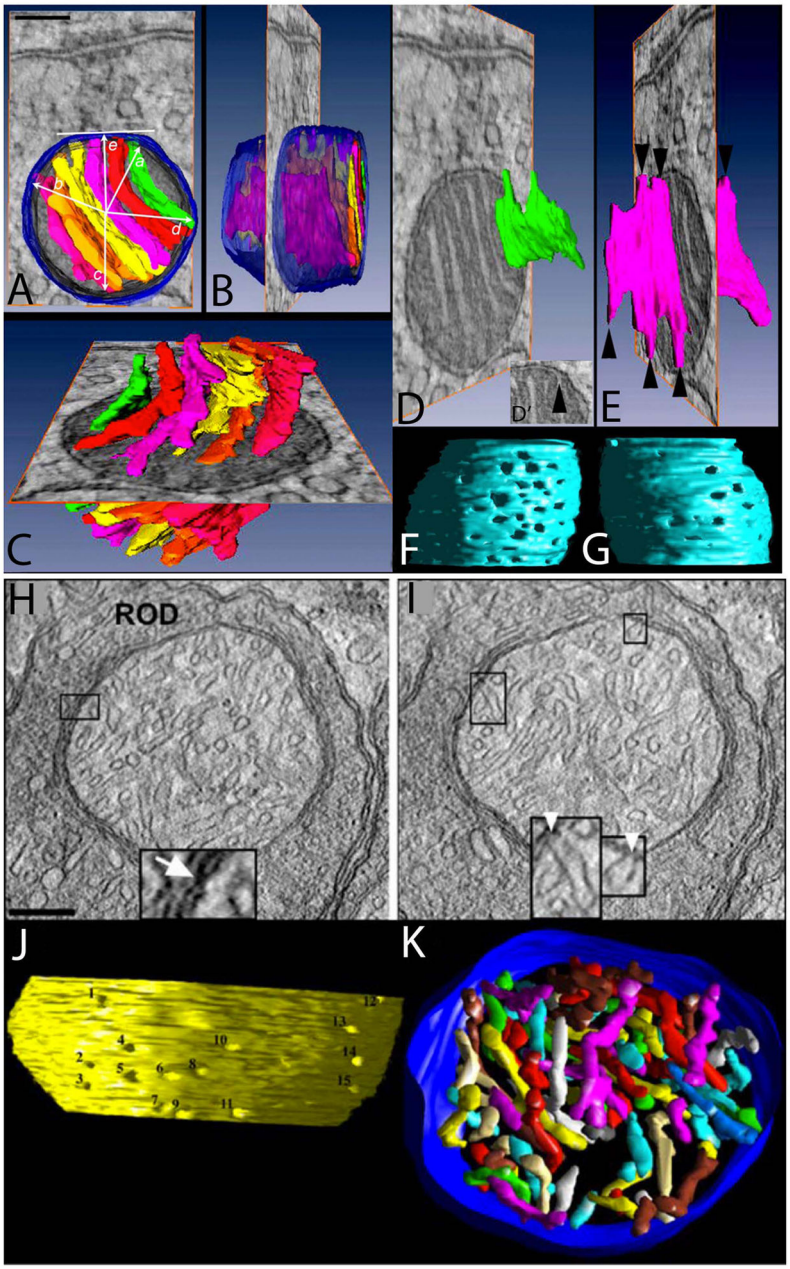

Figure 5. Nerve terminal mitochondria

(A–G). 3D reconstructions of mitochondria in the calyx of Held from tomographic series. **(A–C).** Top-down and side-on views of 3D rendered reconstruction of mitochondrion (outer membrane, blue; cristae, colors) superimposed over virtual ET slice. Mitochondrion together with linking structures and adherens junction (at top of virtual slice) comprise a mitochondria-associated adherens junction (MAC). Angular deviation of cristae junctions relative to vector through middle of mitochondrion and normal to membrane membrane; cristae junctions are not located along the sides of the mitochondrion. Note in (C) individual cristae are not interconnected. Scale bar in A 100 nm. **(D-E).** Single cristae extend tubular structures that link with the intermembrane space through cristae junctions (arrowheads in

D, inset and E). **(F–G).** Views of inner mitochondrial membrane (IMM) with outer mitochondrial membrane (OMM) removed. Note the increased density of cristae junctions found along the presynaptic face in F when compared to the non-synaptic face in G. (A–G) Adapted from (Perkins et al., 2010). **(H–K).** 3D reconstructions of rod spherule mitochondrion from tomographic series. **(H–I).** Virtual slices though mitochondrion illustrates presence of many cristae. Inset in H shows classical contact site between OMM and inner boundary membrane. Insets show cristae junctions (arrowheads). Scale bar 200 nm. **(J).** 3D view of IMM (yellow) with OMM removed. Cristae junctions (numbered) are similar in diameter. **(K).** 3D view of subset of cristae (various colors) which are mostly tubular; OMM is blue. (H–K) Adapted from Johnson et al. (2007).

Table 1

Synaptic Vesicle Diameters

Tissue Processing									
Aldehyde Fixative	**Dehydration**	**Staining**	**Vitrification**		**Synaptic Vesicle Diameter**	**Arrangement Relative to AZ**	**Species**	**Neuron**	**Citation**
+	+	+	−	CAF	38	Not Measured	Rat	Rod bipolar	Graydon et al. 2014
+	+	+	−		40	Not Measured	Mouse	Rod photoreceptor	Zampighi et al. 2011
+	+	+	−		56	Not Measured	Mouse	NMJ	Nagwaney et al. 2009 *
+	+	+	−		34	Not Measured	Frog	Vestibular hair cells	Lenzi et al. 1999
					47.8	Not Measured	Lamprey	Reticulospinal	Gustafsson et al. 2002
+	+	+	−		34	Not Measured	Locust	Ocelar visual neurons	Leitinger et al. 2011
+	+	+	+	CAF + RF/FS	43	Continuous	*C. elegans*	NMJ	Stigloher et al. 2011
−	+	+	+	HPF/FS	42	Not Measured	Mouse	Hippocampal Slice	Siksou et al. 2013
−	+	+	+		45.4	Periodic	Mouse	Hippocampal Slice	Imig et al. 2014 **
−	−	−	+	Cryo ET	39.5	Periodic	Mouse	Cortex Synaptosome	Fernandez- Busnadiego et al. 2010
−	−	−	+		41.5	Periodic	Mouse	Hippocampal Slice	Fernandez- Busnadiego et al. 2010

* unpublished observation that diameters are similar with rapid freezing

** grand average of control animals

Table 2

Synaptic Vesicle Connectors and Tethers

Tissue Processing	Connector Length (nm)	Connectors/Synaptic Vesicle	Species	Neuron	Citation
CAF	< 15	< 12	Lamprey	Reticulospinal Synapse	Gustafsson et al. 2002
	32	2.8	Cat	Calyx of Held	Perkins et al. 2010
	10–20 nm	3–6	Rat	Forebrain and Hippocampal	Burette et al. 2012
CAF + RF/FS	25.1	1	*C. elegans*	Slices NMJ	Stigloher et al. 2011
HPF/FS	32	1.5–1.7	Rat, Mouse	Hippocampal Slice/Culture	Siksou et al. 2007, 2009b
	Yes		*Drosophila*	NMJ	Jiao et al. 2010
Cryo ET	~11	~2.5	Mouse	Cortex Synaptosome	Fernandez-Busnadiego et al. 2010
	Tether Length (nm)	Tethers/ Synaptic Vesicle			
CAF	21		Frog	Vestibular Hair Cell	Lenzi et al. 1999, 2002
	Yes		Rat	Rod Bipolar Cell	Graydon et al. 2014
	8.6	4.1	Frog	NMJ	Szule et al. 2012
HPF/FS	Yes		Rat, Mouse	Hippocampal Slice/Culture Hippocampal	Siksou et al. 2007, 2009b
	Yes		Mouse	Neuron Culture	Arthur et al. 2010
	Yes		*Drosophila*	NMJ	Jiao et al. 2010
Cryo ET	5		Rat	Synaptosome	Fernandez- Busnadiego et al. 2013

"Yes" indicates presence of connectors or tethers without quantitative measurements.